American Mineralogist, Volume 74, pages 513–529, 1989

Solubility of argon in silicate liquids at high pressures*

Bradford S. White**
Department of Earth and Space Sciences, University of California, Los Angeles, Los Angeles, California 90024-1567, U.S.A.
Mark Brearley**
Institute of Geophysics, University of California, Los Angeles, Los Angeles, California 90024-1567, U.S.A.
Art Montana
Department of Earth and Space Sciences and Institute of Geophysics, University of California, Los Angeles, Los Angeles, California 90024-1567, U.S.A.

Abstract

To further our understanding of the relationship between the structure of silicate liquids and the dissolution of molecular species such as H_2O and CO_2 in these liquids, we determined the solubility of Ar in silicate liquids as a function of pressure, temperature, and composition. Liquid Ar, together with the silicate sample, was loaded into Pt capsules in a glove-box under positive Ar-gas pressure. Ar-saturated glasses were synthesized from liquids in piston-cylinder apparatus from 5 to 25 kbar and 1000 to 1750 °C. The concentration of Ar, determined by electron microprobe, increases with pressure to at least 25 kbar. For example, in $KAlSi_3O_8$ liquids at 1600 °C, the concentration of Ar (in wt%) increases from 0.35 ± 0.07 at 9 kbar to 1.28 ± 0.07 at 25 kbar. The solubility of Ar is also strongly dependent on the composition of the liquid. At 15 kbar and 1600 °C, the concentration of Ar is greatest in granitic liquid (0.99 ± 0.11 wt%), followed by liquids of sanidine (0.72 ± 0.04), albite (0.69 ± 0.05), basalt (0.13 ± 0.02), anorthite (0.09 ± 0.01), and diopside (0.04 ± 0.01) composition. Adding SiO_2 to $CaAl_2Si_2O_8$ markedly increases the Ar concentration, suggesting that Ar is most soluble in liquid SiO_2. No systematic trend of solubility with temperature was discerned within the limits of error in the solubility measurements, except in $K_2Si_4O_9$, which has a positive temperature dependence.

An equation of state is used to describe the concentration of Ar as a function of pressure and temperature. The partial molar volume of Ar in the liquid ranges from 20.6 cm^3/mol in $KAlSi_3O_8$ liquid to 23.7 cm^3/mol in basalt, and the molar enthalpies of solution range from 7.2 kcal/mol in $KAlSi_3O_8$ liquid to 12.0 kcal/mol in $K_2Si_4O_9$ liquid. Our determinations of the freezing-point depressions of sanidine, albite, anorthite, and diopside by Ar are in accord with the small depressions calculated using the colligative properties of simple dilute solutions. This supports the assumption that Ar is dissolving as a chemically inert, atomic species.

These data provide insight into the solution of molecular volatile species in silicate liquids. Our measurements indicate that Ar is more soluble in fully polymerized liquids with a high ratio of Si to Al, which is similar to the compositional dependence of the solubility of molecular CO_2 in silicate liquids. The similarities between the compositional trends and the absolute solubilities of Ar and molecular CO_2 suggest that the Ar atom and CO_2 molecule occupy similar sites in the liquid, possibly within clusters of Si tetrahedra. The systematics of the dissolution of molecular H_2O indicate that it behaves quite differently than Ar or molecular CO_2.

Introduction

Volatile components can substantially influence the physical, thermal, and structural properties of silicate liquids. H_2O and CO_2 are important in igneous systems, and this has prompted considerable research into the effects of these components on the properties of silicate liquids. For example, in silicate-H_2O systems, the effect of H_2O on phase relationships (e.g., Goranson, 1938; Boettcher and Wyllie, 1969; Eggler and Rosenhauer, 1978), the solubility and speciation of H_2O in magmas (e.g., Oxtoby and Hamilton, 1978; Stolper, 1982b; Silver and Stolper, 1985; McMillan and Holloway, 1987; Silver, 1988), and the change in liquid viscosity as a result of dissolved H_2O (Shaw, 1963; Dingwell, 1987) have been carefully determined at high pressures. Recent work has focused on the

* Institute of Geophysics and Planetary Physics Contribution Number 3113.

** Present address: (Brearley) Bayerisches Geoinstitut, Universitat Bayreuth, Postfach 10 12 51, 8580 Bayreuth, West Germany; (White) Division of Geological and Planetary Sciences, California Institute of Technology, Pasadena, California 91125, U.S.A.

0003–004X/89/0506–0513$02.00

solution of C in simple silicate-CO_2 systems at high pressure using vapor-saturated freezing-point determinations (Boettcher, 1984; Boettcher et al., 1987), infrared and Raman spectroscopy (Stolper et al., 1987; Fine and Stolper, 1985; Mysen and Virgo, 1980a, 1980b), and the effect of CO_2 on the viscosity of silicate liquids (Brearley and Boettcher, 1986). Other geologically relevant volatiles such as H_2 and F are the focus of similar studies. H_2O, CO_2, H_2, and F are characterized by their chemical reactivity with the silicate liquid, forming ion-complexes or substituting with oxygen in the liquid structure. In contrast, comparatively little is known about the effect of a molecular or atomic species on the properties of silicate liquids at high pressures.

The solubilities of volatiles in silicate liquids and glasses are sensitive to the structure and composition of the solvent. Therefore, knowing the solubility as a function of pressure and composition provides information on the ensuing structural changes in the solvent (e.g., Shelby, 1976). Because of their low reactivity and polarizability (Greenwood and Earnshaw, 1984), it is assumed that the light noble gases dissolve inertly in silicate liquids as an atomic species. The study of a solubility mechanism that does not alter the structure of the liquid by breaking bonds in the silicate framework is important for two reasons. First, the compositional dependence of the solubility can be interpreted in light of our present understanding of the structures of liquids. Second, by measuring the solubility of the light noble gases in silicate liquids and by comparing these data with the effect of the solution of noble gases on the thermodynamic and physical properties of the system, we can better understand the solution process of the molecular components of H_2O and CO_2 in silicate liquids at high pressures and temperatures.

In addition, the noble gases are important constituents of planetary atmospheres ($\sim$1% in the present terrestrial atmosphere) and occur as trace elements in all geologic materials (Ozima and Podosek, 1983). Because of their ubiquity, they serve as indicators of magma petrogenesis, as probes into the internal structure of the Earth, and as clues to the mechanisms governing accretion and formation of the Solar System. An understanding of igneous processes occurring at elevated pressures, such as the equilibrium partitioning of noble gases between solid, liquid, and vapor, and the devolatilization of magmas during ascent requires knowledge of the systematics of magma-volatile interactions. To that extent, research on the solubilities of the noble gases in silicate magmas at the pressures and temperatures in the upper mantle will further our understanding of these processes.

We developed a technique for loading liquid Ar, together with silicate samples, into sealed Pt capsules for experimentation at high pressures (Boettcher et al., 1987). Our method allows us to synthesize Ar-saturated glasses (liquids) at pressures higher than those that have been obtained using Ar gas as the pressure-transmitting medium. The solubility of Ar was determined in eight glasses quenched from silicate liquid compositions at pressures of 5–25 kbar and temperatures of 1000–1750 °C. All compositions contained concentrations of Ar measurable by electron-microprobe analysis. We also determined the Ar-saturated solidi of sanidine, albite, anorthite, and diopside. The observed freezing-point depressions are consistent with those calculated using a simple thermodynamic model applied to our experimental data.

Previous work

Low pressure

The solubilities of the noble gases (except Rn) have been determined in natural magmas at high temperatures and very low gas pressures (e.g., Kirsten, 1968; Jambon et al., 1982; Hayatsu and Waboso, 1985; Hiyagon and Ozima, 1982; Lux, 1987; Broadhurst et al., 1988). In these studies, the noble gases were equilibrated with the molten sample in a controlled-atmosphere furnace. The liquids were quenched and analyzed by stepwise heating and mass spectrometry (Ozima and Podosek, 1983). It has been demonstrated that the solubilities of the noble gases decrease with increasing atomic number of the gas, that the enthalpy of solution is small and positive, and that the solubitities increase as a linear function of pressure in the low-pressure regime (i.e., obey Henry's law; Lux, 1987). Lux (1987) showed that the solubilities of the gases generally decrease with increasing density of the liquid.

Shelby (1972, 1974) conducted an extensive study of the solubilities of the light noble gases (He and Ne) in simple silicate glasses, using them as a probe of the structure of the glass. He concluded that the enthalpy of solution of the light noble gases is small and generally negative, that the solubility is strongly dependent on glass composition (e.g., the solubility decreases as K_2O or Na_2O is added to SiO_2), and that these compositional trends can be rationalized in terms of free-volume theory (Doremus, 1973). In sodium aluminosilicate glasses, increasing the Al/Na ratio from 0 to 1, at a constant silica content, changes the solubility of He in a nonlinear fashion (Shelby and Eagan, 1976), suggesting that the structure of the glass exerts a control on the solubility of He.

High pressure

The extremely low boiling point of Ar (87 K) and the inability of Ar to form dissociable compounds creates difficulties in investigating Ar-silicate systems at high pressures. Consequently, few relevant high-pressure experiments have been conducted, and most have used the noble gases as the pressure-transmitting medium and the solute. Faile and Roy (1966) determined the solubility of noble gases in glasses on the Na_2O-B_2O_3 join and in $K_2Si_4O_9$. Their results indicate that noble gases are highly soluble in glasses at pressures up to 9.5 kbar and that there is a weak positive temperature dependence of the solubility. Shelby (1976) suggested that the pressure dependence of the solubility of He and Ne in SiO_2 glass deviates from Henry's law and is best explained by the

Langmuir equation (Barrer and Vaughan, 1967). Carroll and Stolper (1987) demonstrated that the solubility of Ar in SiO_2 glass is approximated by Henry's law at 0.2–2.8 kbar and 500–800 °C. Their determinations of the percentage of dissolved Ar using an electron microprobe are much lower than those of Faile and Roy (1966) using a weight-loss technique. Roselieb et al. (1988) used Knudsen-cell mass spectrometry to determine the solubilities of noble gases in $NaAlSi_3O_8$ glass at 1000 °C and pressures up to 5 kbar. They confirmed the results of low-pressure experiments that showed that the solubilities of the noble gases decrease with increasing atomic number and obey the Langmuir equation.

Experimental procedure

Starting materials

The albite was from the Franciscan Formation of California (Luth and Boettcher, 1986). Synthetic sanidine was prepared by crystallizing $KAlSi_3O_8$ glass hydrothermally at 2 kbar and 700 °C for 2 weeks. The product was examined optically to ensure complete reaction and verified by X-ray diffraction. Synthetic anorthite was crystallized hydrothermally from a glass at 5 kbar and 1100 °C for 24 h resulting in optically homogeneous, fine-grained anorthite, which was verified by X-ray diffraction. Diopside was prepared by melting dried, reagent-grade oxides at 1 atm and 1450 °C for 8 h, grinding and re-fusing several times (Luth and Boettcher, 1986). The resulting bubble-free glass was crystallized at 1 bar and 1300 °C for 24 h, and then recrystallized hydrothermally at 5 kbar and 1100 °C for 24 h, producing a fine-grained diopside. The intermediate plagioclase was made from a gel (Luth and Ingamells, 1965) and crystallized at 1 bar and 1100 °C. Intermediate compositions on the diopside-albite join are the same glasses used by Scarfe and Cronin (1985) and Brearley et al. (1986). Intermediate compositions on the anorthite-quartz join were made by mixing crystalline anorthite (see above) and natural quartz. The quartz is that used by Boettcher (1984) and Luth and Boettcher (1986). $K_2Si_4O_9$ was prepared by melting decarbonated K_2CO_3 and natural quartz at 1 bar and 1400 °C for 1 h, followed by grinding and re-fusing four times to produce a bubble-free glass. The granite is a biotite granite (Boettcher and Wyllie, 1968) that was dehydrated at 1 bar and 700 °C for 1 week. Optical examination and X-ray diffraction confirmed the absence of hydrous minerals in the starting material. The basalt is an olivine tholeiite from the 1921 Kilauea eruption. All starting materials were finely ground and stored in a vacuum desiccator; their compositions are in Table 1.

Table 1. Compositions of starting materials (wt%)

	1	2	3	4	5
SiO_2	68.48	43.12	55.87	64.75	66.18(71.89)
Al_2O_3	19.30	35.76	27.66	18.03	
Fe_2O_3	0.03			0.02	
FeO		0.05			
CaO	0.01	20.27	10.34		
Na_2O	11.70	0.16	5.95	0.07	
K_2O	0.03			16.52	25.88(28.16)
Total	99.55	99.36	99.82	99.39	92.06

	6	7	8	9	10
SiO_2	55.38	65.65	62.98	59.40	82.39(73.89)
Al_2O_3	0.12	15.48	10.6	25.64	11.36(16.42)
FeO	0.05				
MgO	19.14	3.92	8.15	12.66	
CaO	25.07	5.50	11.81	18.55	6.25(9.08)
Na_2O		9.20	6.70	3.61	
Total	99.76	99.75	100.26	99.86	100.00(99.39)

	11	12	13	14
SiO_2	56.68	66.79	75.40	49.11
TiO_2			0.15	2.51
Al_2O_3	27.27	21.14	13.50	12.74
Fe_2O_3				3.23
FeO			0.64	8.40
MnO			0.04	0.17
MgO	0.13		0.10	10.31
CaO	15.28	11.80	1.00	10.73
Na_2O			4.00	1.97
K_2O	4.60	0.49		
P_2O_5			0.07	0.27
Total	99.36	99.73	99.50	99.93

Note: All analyses by electron microprobe except 13 and 14 (XRF). Columns are as follows: (1) Albite. (2) Anorthite. (3) $Ab_{50}An_{50}$ (mol%). (4) Sanidine. (5) $K_2Si_4O_9$ (low total because of adsorbed H_2O; stoichiometry indicates glass is on composition; numbers in parentheses are normalized to 100%). (6) Diopside. (7) $Di_{25}Ab_{75}$ (mol%). (8) $Di_{50}Ab_{50}$ (mol%). (9) $Di_{75}Ab_{25}$ (mol%). (10) An_5Qz_{91} [(mol%); numbers in parentheses represent glass composition $An_{15}Qz_{85}$ (mol%); this composition did not melt completely and still contained some quartz]. (11) $An_{40}Qz_{60}$ (mol%). (12) $An_{23}Qz_{77}$ (mol%). (13) Granite. (14) Olivine tholeiite.

Capsule loading

Approximately 2–10 mg of starting material were loaded into either a 1.6- or 2-mm-diameter, 10-mm-long Pt capsule and tamped down with a steel rod. The capsule was partially closed by welding at the top and dried for at least 2 h. Glass starting materials were dried at 400 °C to prevent loss of alkalis; crystalline materials were dried at 900 °C. The Ar was loaded as liquid Ar under ~15 psi Ar-gas pressure in a custom-built glove-box to prevent the condensation of unwanted volatiles on the inside of the capsule. To load the samples, Pt capsules (between 8 and 16 in a batch) were placed in the chamber, which contained an arc welder and two Dewars of liquid Ar. The box was sealed and purged for at least 30 min with Ar gas that passed through two columns, one containing KOH and one $CaSO_4$, to remove CO_2, H_2O, and other contaminants.

Capsules were filled by immersing them in a small Dewar of liquid Ar while being held loosely in the welding vice. The capsule was crimped by tightening the vice and was welded shut in a fine stream of N_2 gas to prevent ionization of the Ar gas in the arc (the N_2 was only flowing for the few seconds it took to weld the capsule). After the capsules were removed from the glove-box, they were weighed to determine the amount of Ar present, adjusting for Pt lost during welding. We commonly encapsulated 2–3 mg of Ar; amounts greater than about 5 mg caused

TABLE 2. Experimental results for the solubility of Ar

Run	*P* (kbar)	*T* (°C)	Duration (min)	Results	Ar (wt%)
				I. $NaAlSi_3O_8$-Ar	
530	9	1350	3	L + V	0.42 ± 0.07
547	9	1500	30	L + V	0.42 ± 0.04
478	12	1350	900	L + V	0.54 ± 0.02
489	12	1400	120	L + V	0.57 ± 0.03
448	12	1500	30	L + V	0.56 ± 0.04
490	12	1600	3	L + V	0.58 ± 0.05
278	15	1350	480	L + V	0.66 ± 0.05
291	15	1400	30	L + V	0.69 ± 0.04
451	15	1500	30	L + V	0.73 ± 0.04
531	15	1500	30	L + V	0.71 ± 0.04
306	15	1600	10	L + V	0.69 ± 0.05
292	20	1400	120	(Ab) + L + V	0.93 ± 0.09
548	20	1400	1440	L + V	0.95 ± 0.07
293	20	1500	30	L + V	0.93 ± 0.05
549R	20	1500	60	L + V	0.95 ± 0.04
296	20	1600	10	L + V	0.92 ± 0.04
280	25	1400	1440	L + V	1.12 ± 0.05
295	25	1500	30	L + V	1.11 ± 0.07
294	25	1600	10	L + V	1.07 ± 0.06
				II. $CaAl_2Si_2O_8$-Ar	
426	9	1600	<1	Co + L + V	0.05 ± 0.02
420	12	1600	3.5	Co + L + V	0.07 ± 0.02
429	12	1700	2	Co + L + V	0.08 ± 0.02
400	15	1600	15	Co + qAn + L + V	0.09 ± 0.01
403	20	1600	6	Co + L + V	0.12 ± 0.04
428	20	1700	2	Co + L + V	0.12 ± 0.02
427	25	1600	5	Co + qAn + L + V	0.14 ± 0.02
				III. $Ab_{50}An_{50}$-Ar	
551	9	1600	<1	L + V	0.18 ± 0.09
541	12	1600	5	L + V	0.24 ± 0.02
499	15	1500	120	qPl + L + V	0.28 ± 0.02
539	15	1600	20	L + V	0.30 ± 0.03
501	20	1600	20	(Co) + L + V	0.37 ± 0.04
540	25	1600	20	Co + L + V	0.44 ± 0.03
				IV. $CaMgSi_2O_6$-Ar	
233	9	1600	<1	L + V	0.01 ± 0.01
224	12	1600	1	L + V	0.03 ± 0.01
162	15	1610	10	L + V	0.04 ± 0.01
223	20	1675	1	(Di) + L + V	0.05 ± 0.01
220	25	1750	<1	L + V	0.08 ± 0.02
				V. $KAlSi_3O_8$-Ar	
515	5	1500	<1	L + V	0.17 ± 0.03
437	9	1500	10	L + V	0.34 ± 0.08
513	9	1600	<1	L + V	0.35 ± 0.07
512	12	1400	5	L + V	0.58 ± 0.10
421	12	1500	7	L + V	0.53 ± 0.03
440	12	1600	10	L + V	0.56 ± 0.06
412	15	1500	60	L + V	0.77 ± 0.05
455	15	1600	10	L + V	0.72 ± 0.04
517	15	1700	5	qSa + L + V	0.71 ± 0.12
422	20	1500	30	L + V	1.03 ± 0.08
454	20	1600	10	L + V	1.06 ± 0.08
439	20	1700	3	L + V	1.06 ± 0.11
4382	5	1600	10	L + V	1.28 ± 0.07
				VI. Granite-Ar	
520	9	1500	<1	Qz + L + V	0.34 ± 0.09
521	12	1500	120	L + V	0.77 ± 0.05
474	15	1400	60	Qz + L + V	0.89 ± 0.07
477	15	1500	120	(Qz) + L + V	0.93 ± 0.08
519	15	1600	5	(Qz) + L + V	0.99 ± 0.11
475	20	1500	120	(Qz) + L + V	1.28 ± 0.09
476	25	1500	120	(Qz) + L + V	1.54 ± 0.10
546	25	1600	30	Xl + L + V	1.45 ± 0.12
				VII. Basalt-Ar	
525	9	1500	<1	L + V	0.07 ± 0.02
524	12	1500	60	L + V	0.11 ± 0.03
471	15	1400	60	(Ol) + L + V	0.11 ± 0.02
473	15	1500	120	L + V	0.13 ± 0.02
526	15	1600	4	L + V	0.13 ± 0.02
472	20	1500	120	L + V	0.15 ± 0.02
523	25	1500	120	L + V	0.18 ± 0.02
522	25	1600	10	L + V	0.20 ± 0.02
				VIII. $K_2Si_4O_9$-Ar	
494	9	1000	1440	L + V	0.35 ± 0.03
511	9	1200	1440	(Xl) + L + V	0.41 ± 0.03
504	9	1400	30	L + V	0.56 ± 0.06
496	12	1200	240	(Xl) + L + V	0.57 ± 0.04
503	12	1400	120	L + V	0.27 ± 0.04
497	15	1200	1080	L + V	0.68 ± 0.03
506	15	1200	1440	L + V	0.70 ± 0.07
510	15	1400	120	L + V	0.85 ± 0.04
505	20	1200	1440	L + V	0.99 ± 0.06
509	20	1400	240	(Xl) + L + V	1.12 ± 0.08
508	25	1200	1440	L + V	1.18 ± 0.05
507	25	1400	120	L + V	1.33 ± 0.07
543	25	1600	30	L + V	1.57 ± 0.09
				IX. $Di_{25}Ab_{75}$-Ar	
553	15	1600	20	L + V	0.44 ± 0.03
				X. $Di_{50}Ab_{50}$-Ar	
538	15	1600	20	L + V	0.24 ± 0.02
				XI. $Di_{75}Ab_{25}$-Ar	
537	15	1600	20	L + V	0.12 ± 0.02
				XII. $An_{40}Qz_{60}$-Ar	
532	15	1600	10	L + V	0.21 ± 0.03
				XIII. $An_{23}Qz_{77}$-Ar	
534	15	1600	10	L + V	0.42 ± 0.05
				XIV. $An_{15}Qz_{85}$-Ar	
536	15	1700	8	Qz + L + V	0.60 ± 0.08

Note: L = liquid, V = vapor, R = reversal (run held at 25 kbar and 1500 °C for 30 min, then dropped to 20 kbar and 1500 °C for 30 min), Ab = albite, Co = corundum, Di = diopside, Qz = quartz, Ol = olivine, Xl = crystals of undetermined composition, qAn = quench anorthite, qPl = quench plagioclase, qSa = quench sanidine. Phases in parentheses are present in trace amounts. Errors on concentration of dissolved Ar discussed in text.

the capsule to explode. We attained Ar pressure as high as 125 bars in some of our charges.

Each capsule was sealed into a 3- or 3.5-mm-diameter Pt capsule along with 100–200 mg of sintered hematite. The hematite reacted to form magnetite + H_2O during the run and buffered the f_{H_2} at very low values. Al_2O_3 was used instead of hematite in experiments with diopside at pressures greater than 15 kbar to prevent the liquid from quenching to diopside (Boettcher et al., 1982). These runs were very short in duration (Table 2) and may not be greatly affected by the lack of a H_2 buffer.

Run procedure

All experiments were performed in piston-cylinder apparatus, with 2.54-cm furnace assemblies composed of NaCl, pyrex, graphite, BN, and MgO (Boettcher et al., 1981). The capsules were run horizontally, with temperature monitored by $Pt\text{-}Pt_{90}Rh_{10}$ thermocouples (encased in 99.8% alumina ceramic) in contact with the top of the capsule. The hot piston-in technique was used to bring the experiments to run conditions, increasing the pressure

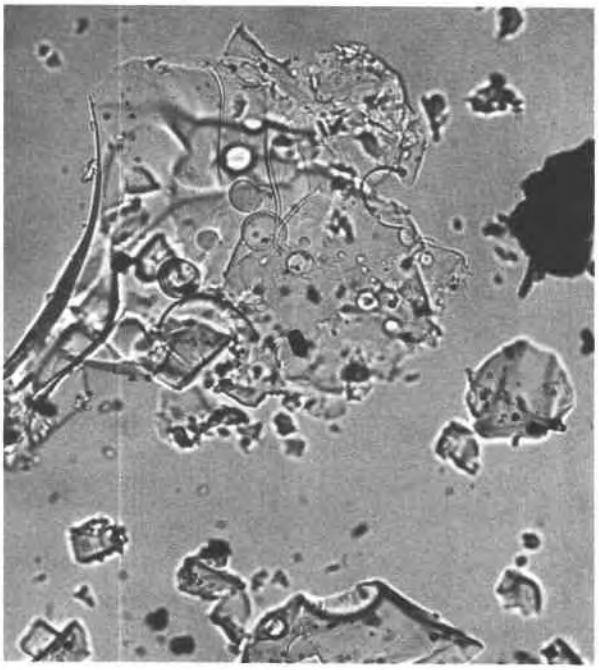

Fig. 1. Photomicrograph of Ar-saturated $NaAlSi_3O_8$ glass. The glass chip is ~50 μm wide.

Table 3. Definitive solidus experiments

Run	*P* (kbar)	*T* (°C)	*t* (min)	Ar* (wt%)	Results
			I. $NaAlSi_3O_8$-Ar		
247	15	1200	1440	50.3	Ab + V
242	15	1210	1440	30.0	Ab + L + V
264R	15	1230	360	31.1	
		1200	1440		Ab + V
2008**	16	1230	1200	0	Ab
2009**	16	1240	1080	0	Ab + qAb
284	25	1330	1440	22.8	Ab + V
285	25	1350	1260	52.7	Ab + L + V
			II. $CaMgSi_2O_6$-Ar		
156	15	1560	10	3.5	Di + V
154	15	1570	10	7.6	qDi + L + V
140	15	1560	5	0	Di
142	15	1570	5	0	Di + qDi
			III. $CaAl_2Si_2O_8$-Ar		
436	18.2	1530	30	40.1	An + Co + V
435	18.2	1540	30	26.2	An + Co + L + V
570	18.2	1540	30	0	An + Co
571	18.2	1550	30	0	An + Co + L
			IV. $KAlSi_3O_8$-Ar†		
563	5	1140	360	37.2	Sa + V
564	5	1150	360	34.7	Sa + L + V
562	12	1290	360	39.0	Sa + V
557	12	1300	360	45.9	Sa + L + V
446	20	1410	360	29.4	Sa + V
444	20	1420	360	64.9	Sa + L + V

Note: L = liquid, V = vapor, Ab = albite, Di = diopside, An = anorthite, Co = corundum, Sa = sanidine, q = quench.

* Ar refers to the approximate calculated percentage of vapor from the weight difference before and after loading the Ar.

** Vapor-absent melting of albite at 16 kbar from Boettcher et al. (1982).

† See Fig. 11 for vapor-absent melting of sanidine.

to 90% of the final pressure, increasing the temperature to 90% of the final temperature, and then increasing the pressure and finally the temperature to the final values. The pressure was controlled to ±0.1 kbar, and the temperature to ±3 °C. The experiments were terminated by shutting off the power to the furnace, resulting in quench rates of at least 150–200 °C/s.

The outer capsule was weighed, punctured, and reweighed to check if Ar had leaked from the sample capsule before or during the experiment. The buffer was removed from the sample capsule and examined optically to ensure that >50% hematite remained in the buffer. The sample capsule was then weighed, punctured, and reweighed to demonstrate retention of Ar during the run.

Run products were examined optically for bubbles and to estimate the percentage of liquid. In most cases, the products were 100% quenched liquid (glass) containing bubbles of various sizes depending on the pressure and composition (i.e., depending on the viscosity of the liquid). Some runs either showed devitrification of the glass after the run or were not completely molten (Table 2). Figure 1 displays the typical appearance of an Ar-saturated glass. The bubbles visible in Figure 1 are large enough to be avoided during the microprobe analysis and range in size from 3 to 20 μm. Although we examined each sample with a petrographic microscope, the presence of submicroscopic bubbles cannot be ruled out.

We used two methods to demonstrate equilibrium solubility. For example, we conducted a run (no. 548, Table 2) with albite liquid at 20 kbar and 1400 °C for 24 h that resulted in an identical concentration of dissolved Ar as a run for 4 h (run 292). Second, we conducted an experiment (run 549) at 25 kbar and 1500 °C for 30 min and then lowered the pressure to 20 kbar for 30 min, keeping the temperature constant. The concentration of Ar was indistinguishable from that in a run at 20 kbar, 1500 °C (run 293, Table 2).

Experiments designed to locate the Ar-saturated solidus were performed in the same manner as those previously described. The criterion for identifying the onset of melting was the presence of glass (quenched liquid) in the run products. To demonstrate the attainment of equilibrium, the solidi were reversed in two-stage experiments. First, we placed the sample at *P-T* conditions known from previous experiments to melt the sample. After sufficient time to melt the sample, the temperature was dropped to subsolidus conditions, again determined from previous experience. The absence of glass confirms equilibrium. Details of the experiments are given in Table 3.

Microprobe analysis

With the electron microprobe, we determined the compositions of the glasses and the concentrations of dissolved Ar in the glasses. The concentrations of the major elements were indistinguishable from those of the starting materials except for one composition on the anorthite-quartz join that did not melt completely; this composition is also in Table 1. Postrun glass compositions of

$K_2Si_4O_9$ were difficult to obtain because of the hygroscopic nature of the glass and partial devitrification in some cases. There was no apparent preferential loss of K from the glass with increasing temperature, ruling out partitioning of K into the vapor phase as a reason for the temperature dependence of the solubility of Ar for this system. For anorthite bulk compositions, the liquid composition changes with pressure as a result of the incongruent melting of anorthite to corundum + liquid at pressures >9 kbar (Boettcher, 1970; Goldsmith, 1980), resulting in a liquid whose CaO and SiO_2 contents are enriched and whose Al_2O_3 content is depleted relative to $CaAl_2Si_2O_8$. However, these compositional changes are unlikely to change the concentration of dissolved Ar by a significant amount, considering the low solubility of Ar in this liquid (Table 2).

In the absence of a reliable standard material for Ar, the concentrations of dissolved Ar in the glasses were determined by a technique using a calibration curve. Operating conditions were 15-kV accelerating voltage, 12-nA beam current, a 10-μm beam diameter, and 40-s counting times on peak and background positions. When the sample was viewed in the transmitted light mode, it was possible to locate surface and subsurface bubble-free glass of sufficient size to accommodate the 10-μm beam. The number of counts for the elements adjacent to Ar in the periodic table were determined on standards of known composition: pyrite (S), NaCl (Cl), orthoclase (K), and grossular (Ca). These were used to calculate the counts for the pure element and were plotted against atomic number (Fig. 2). The counting rate for 100% Ar was calculated by least-squares regression of the counting rates for pure S, Cl, K, and Ca (Fig. 2). Because the counts for K lie below the fitted line and those for Ca lie above, we assigned an error to the counts for Ar by passing a line through the upper error bracket ($\sqrt{N}$) for K and the lower error bracket for Ca (Fig. 2). This resulted in an error of 2–2.5% for Ar, depending on the errors associated with the counting statistics for K and Ca. The calibration curve was highly reproducible during the course of a day and from day to day, giving us confidence that this technique is reliable. The counting rates for K and Ca relative to the regressed calibration line always behave in the same manner. The trend in Figure 2 may not be linear and/or the ZAF corrections, which we have ignored, may affect the results. However, the error we assigned should encompass these uncertainties. We tested the calibration curve by analyzing USGS standard W-1 diabase glass for K_2O. The recommended value for K_2O is 0.64 wt% (Flanagan, 1973). Our value for K_2O using the calibration curve is 0.63 ± 0.06 wt% (average of ten analyses), and we obtained a value of 0.66 ± 0.03 wt% (average of three analyses) by quantitative wavelength-dispersive analysis. It is clear that our calibration technique is a credible method of analysis for small elemental concentrations and that ignoring the matrix corrections at these low amounts does not affect the results beyond the error that we have assigned to the analyses. We believe that this accuracy also applies to the measurement of low concentrations of dissolved Ar.

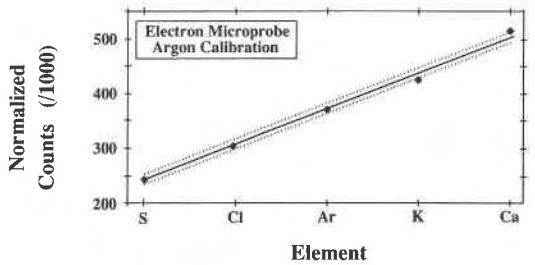

Fig. 2. Counting rate normalized to 100% concentration vs. atomic number for elements adjacent to Ar in the periodic table. See text.

The peak position for Ar X-rays was determined by using a high beam current (>60 nA) on one of our glasses known to contain an appreciable amount of dissolved Ar. We were careful to avoid bubbles and/or crystalline material during analysis, using transmitted and reflected light to ensure that the sample spot was free of bubbles throughout the thickness of the grain. A typical energy-dispersive spectrum for albite glass saturated with Ar is shown in Figure 3, and Figure 4 is a backscattered-electron photograph and an Ar$K\alpha$ X-ray image illustrating the difference in concentration of Ar between albite liquid and crystalline albite from an experiment close to the vapor-saturated solidus. Figure 4 shows that Ar is uniformly distributed in the glass and does not reside in large bubbles.

At least six points were analyzed in each glass. The concentration of Ar was calculated by dividing the average counts ($\pm 2\sigma$) by the counts for 100% Ar from the calibration-curve standardization. The error associated with the concentration of Ar was calculated by adding the 2σ error on the sample counts to that determined from the calibration, resulting in an error ranging from 4 to 100%, depending on the analytical precision and absolute concentration of Ar.

Results

The conditions of the experiments and the concentrations of dissolved Ar are listed in Table 2 and portrayed in Figures 5 to 9. Our choice of liquid compositions allows us to evaluate the compositional dependence of the solubility of Ar as a function of pressure and temperature. Figure 5 illustrates that the increase in concentration of Ar with increasing pressure is approximately linear for all compositions. The solubility of Ar is independent of temperature within experimental uncertainty (Fig. 6A), with the exception of $K_2Si_4O_9$, which shows an isobaric increase in Ar solubility with increasing temperature (Fig. 6B).

Albite-anorthite. Figure 7 shows the isothermal variation in Ar concentration as a function of pressure and composition in plagioclase. The solubility of Ar rapidly

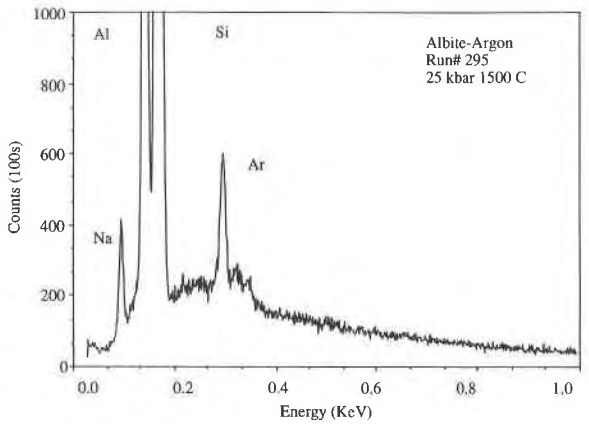

Fig. 3. Energy-dispersive spectrum of Ar-saturated $NaAlSi_3O_8$ glass. The Ar peak height corresponds to 1.11 ± 0.07 wt% Ar.

increases with the addition of $NaAlSi_3O_8$ to $CaAl_2Si_2O_8$ liquid. At 15 kbar and 1600 °C, the concentration of Ar increases from 0.09 ± 0.01 wt% in $CaAl_2Si_2O_8$ liquid to 0.69 ± 0.05 wt% in $NaAlSi_3O_8$ liquid. In $Ab_{50}An_{50}$, the concentration of Ar is less than that expected from a mechanical mixture of the end-members (depicted as a straight line between end-member compositions). Liquids along this join are fully polymerized (e.g., Taylor and Brown, 1979) with no nonbridging oxygens (i.e., NBO/T = 0, Mysen et al., 1982). The Al/Si ratio decreases and the viscosity increases as the liquid composition progresses away from $CaAl_2Si_2O_8$.

Anorthite-quartz. In similar fashion to $NaAlSi_3O_8$-$CaAl_2Si_2O_8$, the $CaAl_2Si_2O_8$-Si_4O_8 join is one of invariant NBO/T = 0. Figure 8 shows that addition of Si_4O_8 component to $CaAl_2Si_2O_8$ results in an increase in Ar solubility at 15 kbar and 1600 °C from 0.09 ± 0.01 wt% in $CaAl_2Si_2O_8$ to 0.60 ± 0.08 wt% in $An_{15}Qz_{85}$ ($An_{15}Qz_{85}$ was run at 1700 °C to compensate for its high melting temperature). At constant pressure and temperature, the viscosities of liquids in this system dramatically increase with decreasing Al/Si, reflecting a change in the geometry of the tetrahedral rings in the liquid (Seifert et al., 1982). Because of the high melting temperature of pure SiO_2, we were unable to obtain data for the quartz end-member. The shape of the solubility vs. composition curve in Figure 8 suggests that the solubility in Ar in a pure SiO_2 liquid is very high.

Albite-diopside. We chose this binary join because the structural-compositional parameter NBO/T increases from 0 for $NaAlSi_3O_8$ to 2 for $CaMgSi_2O_6$, reflecting a progressive depolymerization of the liquid with decreasing $NaAlSi_3O_8$ component (see Brearley et al., 1986, for discussion). At 15 kbar and 1600 °C, the solubility of Ar decreases from 0.69 ± 0.05 wt% in $NaAlSi_3O_8$ to 0.04 ± 0.01 wt% in $CaMgSi_2O_6$ (Fig. 9). The concentrations of Ar in the intermediate compositions along the join represent a negative deviation from a mechanical mixture.

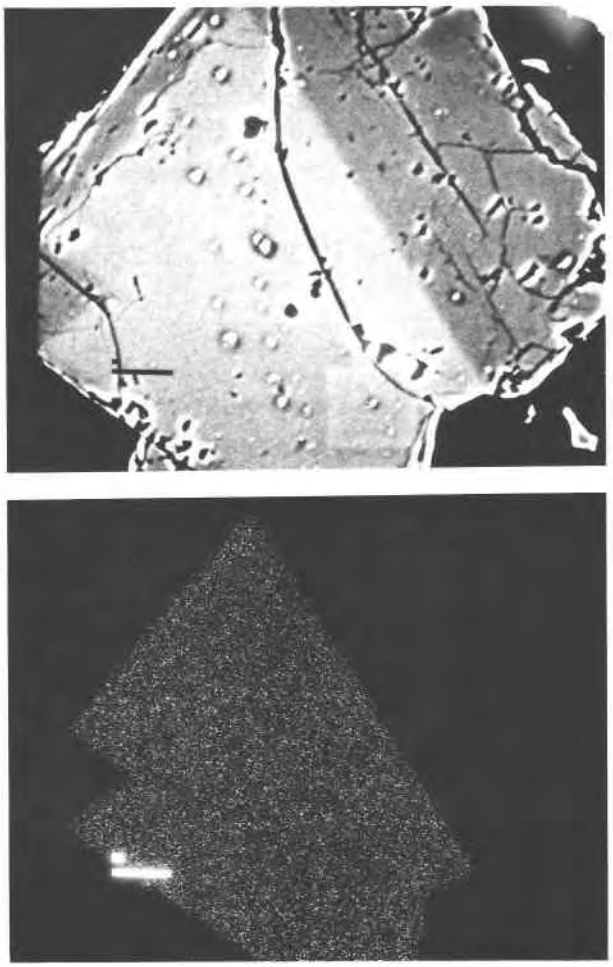

Fig. 4. (**A**, top) Backscattered-electron photograph of Ar-saturated $NaAlSi_3O_8$ glass (light-colored) and albite (dark). (**B**, bottom) Ar X-ray dot image of the above sample. The large scale bars in each case correspond to 10 μm.

$KAlSi_3O_8$ and $K_2Si_4O_9$. We are interested in sanidine and potassium tetrasilicate liquid for several reasons. First, as Al_2O_3 is subtracted from $KAlSi_3O_8$ to form $K_2Si_4O_9$, the NBO/T increases from 0 to 0.5 and the liquid depolymerizes, resulting in a decrease of the viscosity (Dickinson and Scarfe, 1985; White and Montana, unpublished data). This relationship between structure and viscosity is different from the albite-diopside join in that the viscosity of the liquid decreases with increasing mole fraction of silica. Second, Boettcher et al. (1987) showed that CO_2 is much more effective in depressing the freezing point of sanidine than it is in depressing the freezing point of albite or anorthite. On the basis of their determinations of feldspar phase equilibria and the spectroscopic data of Fine and Stolper (1985), Boettcher et al. (1987) proposed that most of the C in $KAlSi_3O_8$ liquid was dissolving as CO_3^{2-}, forming K_2CO_3 complexes and subsequently changing the thermal and structural properties of $KAlSi_3O_8$ liquid. An atomic species such as Ar provides

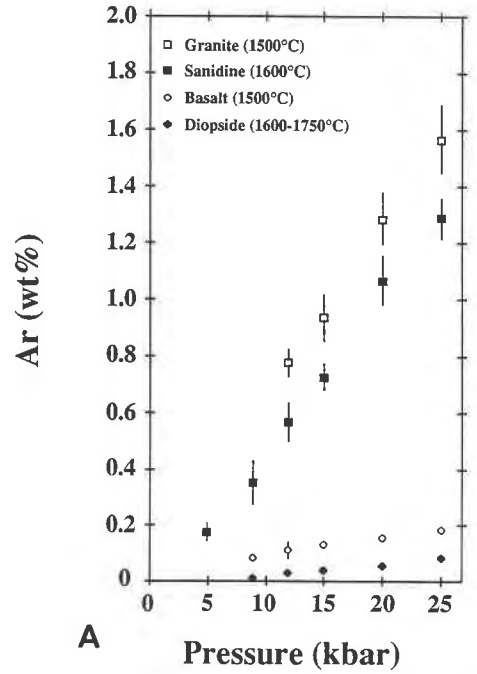

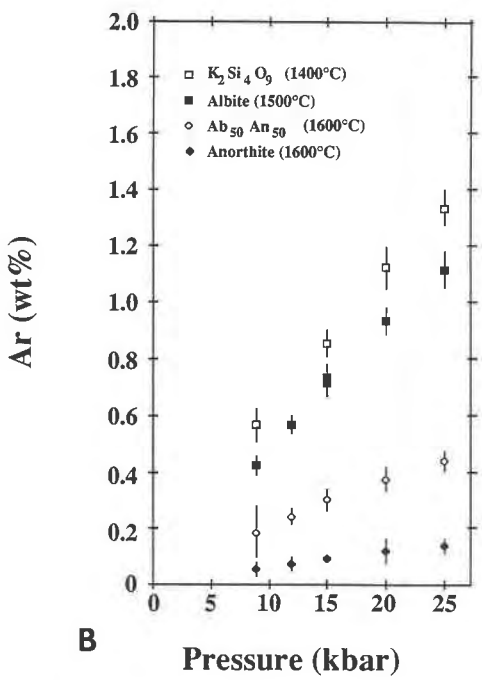

Fig. 5. Concentration of Ar vs. pressure. Errors are discussed in the text and listed in Table 2. Uncertainty in the values without error bars are smaller than the symbols.

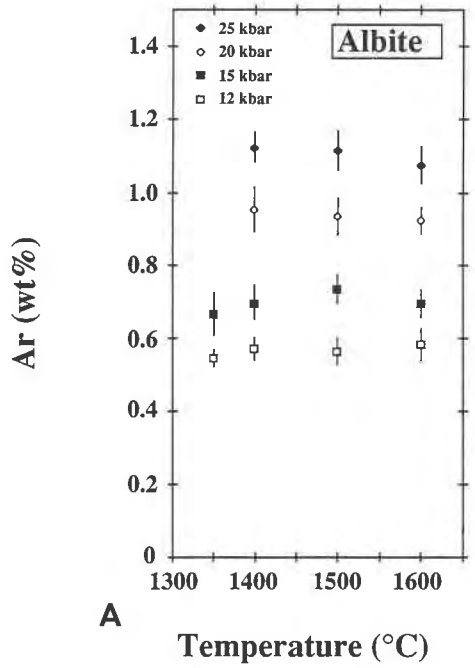

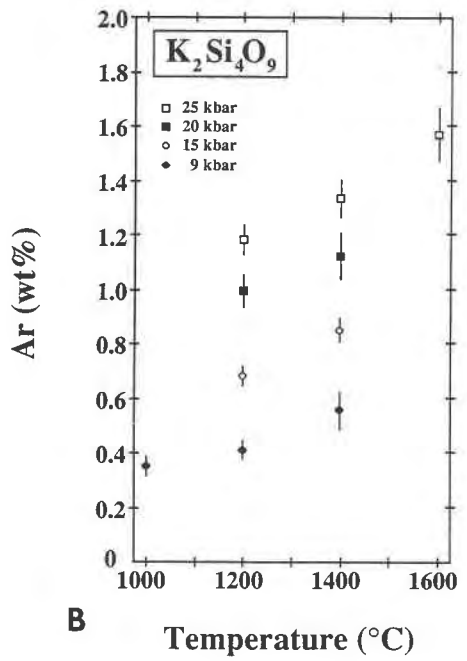

Fig. 6. Concentration of Ar vs. temperature in (**A**) $NaAlSi_3O_8$ glass. (**B**) $K_2Si_4O_9$ glass.

a test of this hypothesis. Finally, Faile and Roy (1966) measured the solubility of Ar in potassium tetrasilicate glass in the pressure range 0–9.5 kbar and at 800 °C and obtained very high solubilities of Ar that are discrepant with our measurements.

The results for $KAlSi_3O_8$ and $K_2Si_4O_9$ are shown in Figure 5 as a function of pressure and in Figure 6 as a function of temperature. Ar is more soluble in $KAlSi_3O_8$ liquid than it is in the other molten feldspars, but $NaAlSi_3O_8$ is considerably closer to $KAlSi_3O_8$ in its ability to dissolve Ar than it is to $CaAl_2Si_2O_8$. For example, at 25 kbar and 1600 °C, $NaAlSi_3O_8$ and $KAlSi_3O_8$ dissolve 1.07 ± 0.06 and 1.28 ± 0.07 wt% Ar, respectively, whereas liquid anorthite contains only 0.14 ± 0.02 wt%

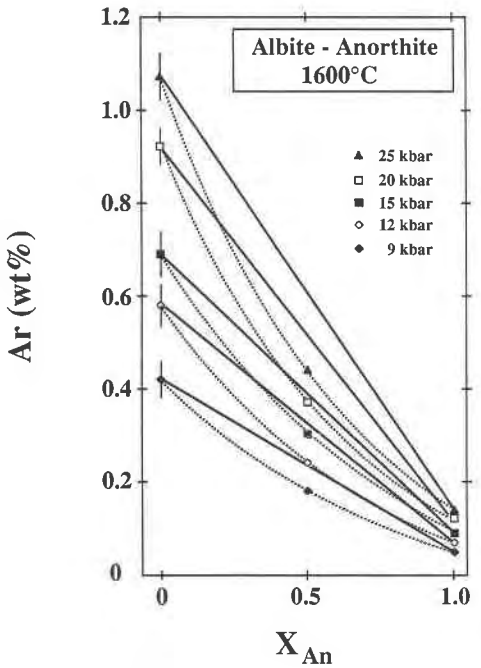

Fig. 7. Concentration of Ar in glasses along the join $NaAlSi_3O_8$-$CaAl_2Si_2O_8$. The solid lines represent a mechanical mixture of the two end-members at each pressure. Some error bars omitted for clarity.

Ar at the same conditions. $K_2Si_4O_9$ recorded the highest Ar concentration (1.57 wt%, 25 kbar, 1600 °C), and it is the only liquid composition in which the solubility of Ar has a detectable temperature dependence.

Granite and basalt. Because basaltic magmas are so common at the Earth's surface, previous attention has focused on the solubility of Ar in basaltic to andesitic composition liquids at low pressure (e.g., Hayatsu and Waboso, 1985; Lux, 1987). Several workers have determined the concentrations of the noble gases in deep-sea basalt glasses (Dymond and Hogan, 1973; Kirsten et al., 1981; Ozima and Zashu, 1983) and granites (Kuroda et al., 1977). Gas concentrations similar to those in igneous rocks can be produced with equilibrium solution of noble gases at atmospheric pressures (Ozima and Podosek, 1983), but it is of geologic interest to ascertain the solubility of these gases in a magma chamber at depth within the Earth. The solubilities of Ar in granite and basalt magmas as a function of P and T follow a pattern expected from observations of their simple silicate analogues. Ar dissolves in granite (highly polymerized, viscous, and high in silica) in concentrations similar to that in alkali feldspars, whereas basalt, with a low viscosity and high normative anorthite and clinopyroxene components, had low concentrations of Ar (Fig. 5). Extrapolation of Hayatsu and Waboso's (1985) Henry's-law constant for Ar in a tholeiitic basalt up to the high pressures of our study, although probably not thermodynamically valid, yields concentrations similar to ours.

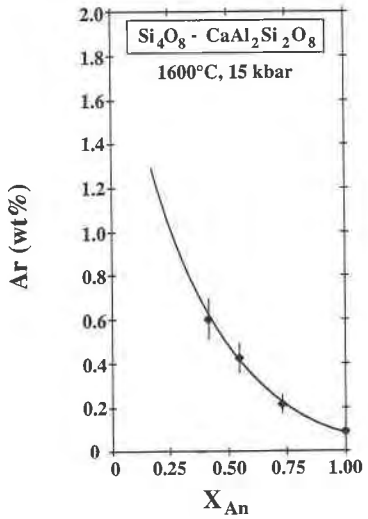

Fig. 8. Concentration of Ar in glasses along the join Si_4O_8-$CaAl_2Si_2O_8$. The data at $X_{An} = 0.41$ were obtained from a glass synthesized at 1700 °C.

Ar as a solute vs. Ar in bubbles? A common problem in the analysis of gases in glasses is the elimination of bubbles from the measurement. Our most viscous liquids, i.e., granite, $NaAlSi_3O_8$, and $KAlSi_3O_8$, contain bubbles or vesicles visible through the petrographic microscope (Fig. 1). In general, the density of bubbles is inversely proportional to pressure, as is the viscosity for these polymerized liquids. Because of the rapid quench, our well-behaved trends of Ar concentration vs. pressure and composition, and the temperature independence of

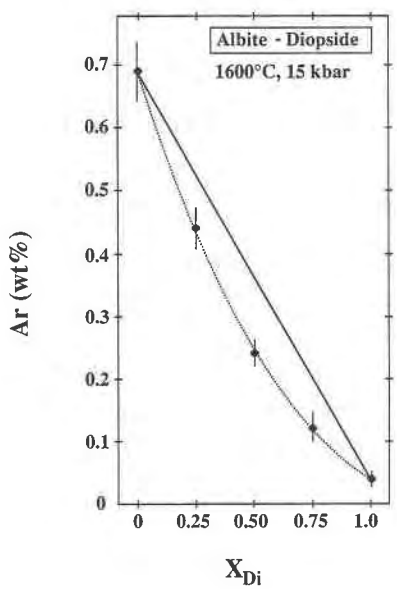

Fig. 9. Concentration of Ar in glasses along the join $NaAlSi_3O_8$-$CaMgSi_2O_6$. The solid line connecting the end-members represents a mechanical mixture of the two end-members.

Ar concentration in the glass in most cases, we feel that these bubbles are not a consequence of Ar exsolution on the quench but result from entrapment of vapor in the viscous liquid. The optical quality of the microscope on the microprobe is sufficient to detect bubbles in the vicinity of the beam so as to exclude them from the analysis. On several occasions we were able to intentionally "drill" into a bubble with the electron beam to produce a large increase in the Ar peak on the energy-dispersive spectrum and a radical increase in the counting rate. Whether the Ar solute resides in nanometer-sized holes as two or more atoms cannot be verified in our study and may be solely a semantic argument (Stolper et al., 1987). The molecular-dynamics simulations of Angell et al. (1988) indicate that some of the Ar in a silicate liquid will be found as pairs occupying "bubbles." Unlike mass-spectrometer techniques that measure Ar adsorbed onto grain surfaces (Lux, 1987), the microprobe method acquires data from grain interiors, eliminating those effects.

Thermodynamics

Solubility

A goal of this research is to observe changes in the thermal and physical properties of silicate liquids as a result of dissolved molecular species. H_2O and CO_2 react with the liquid as illustrated by the following:

$$2H_2O_{(v)} + O^{2-}_{(l)} = H_2O_{(l)} + 2OH^-_{(l)} \quad (1)$$

$$2CO_{2(v)} + O^{2-}_{(l)} = CO_{2(l)} + CO^{2-}_{3(l)} \quad (2)$$

where the subscripts *v* and *l* refers to the vapor and liquid, respectively. These reactions produce significant alterations in the structure of the liquid's (Si,Al)–O tetrahedral network and, concomitantly, adjustments in the thermal and physical properties. Such changes are manifested in new liquidus phase relations (e.g., Kushiro, 1975; Mysen and Boettcher, 1976; Eggler, 1978), by a depression in the freezing point of the crystalline solid (e.g., Bohlen et al., 1982; Boettcher et al., 1987), by a decrease in the viscosity of the liquid (Brearley and Boettcher, 1986; Dingwell, 1987), and a new spectroscopic signature of the glassy silicate (e.g., Mysen and Virgo, 1980a; Stolper, 1982a). What effect, if any, will a solute that dissolves solely as an atomic species have on the above properties?

Silver and Stolper (1985) and Stolper et al. (1987), respectively, developed thermodynamic models for the dissolution of H_2O and CO_2 in silicate liquids based on data acquired by infrared spectroscopy. In their models, the heterogeneous equilibria between H_2O or CO_2 molecules in the vapor and molecular H_2O or CO_2 in the liquid are considered separately from the homogeneous equilibria between the dissolved volatile components and the liquid. The utility of this scheme has been demonstrated by the successful calculation of experimentally determined phase equilibria. Because we are interested in the equilibrium

$$\mu^v_{Ar} = \mu^l_{Ar} \quad (3)$$

and wish to compare our results for dissolved Ar with analogous data for dissolved molecular CO_2 and H_2O, we are utilizing the equation for the heterogeneous vapor-liquid equilibrium derived in Stolper et al. (1987).

After modification, the condition of equilibrium given in Equation 3 becomes:

$$\ln\left(\frac{X_{Ar} f^0_{Ar}}{X^0_{Ar} f_{Ar}}\right) = -\left(\frac{\Delta H^0_{Ar}}{R}\right)(1/T - 1/T^0) - \left(\frac{V^0_{Ar}}{RT}\right)(P - P^0). \quad (4)$$

The superscript ^{0} refers to a standard reference state arbitrarily chosen to be 15 kbar and 1600 °C for each silicate system (except $K_2Si_4O_9$, 15 kbar and 1400 °C). The mole fraction of Ar in the liquid, (X^0_{Ar} and X_{Ar}) is based on the number of moles of Ar in the liquid divided by the sum of the molar amounts of Ar + O^{2-} (Fine and Stolper, 1985). The variable f_{Ar} is the fugacity of Ar in the vapor at *P* and *T* calculated using the modified Redlich-Kwong equation of state (Holloway, 1977; Ferry and Baumgartner, 1987) using data for the corresponding-states parameters for Ar from Chao and Greenkorn (1968); V^0_{Ar} is the standard-state molar volume of Ar in the liquid; ΔH^0_{Ar} the molar enthalpy of solution of Ar at the reference pressure and temperature. Equation 4 assumes that Ar mixes ideally in the liquid (i.e., $a_{Ar} = X_{Ar}$), that V^0_{Ar} is independent of *P* and *T*, and that ΔH^0_{Ar} is independent of temperature. For a more complete description of the assumptions and derivations, see Stolper et al. (1987).

If the concentrations of Ar in the quenched glasses are equivalent to those in the liquid at *P* and *T*, then we can calculate values for X^0_{Ar} and X_{Ar}. Substitution of the other parameters into Equation 4 provides an equation of state to calculate the solubility of Ar at any *P* and *T*. Values of V^0_{Ar} and ΔH^0_{Ar} are determined for each composition by using a multiple variable, linear, least-squares regression program; they are listed in Table 4. In general, the molar volumes are reasonable in that they are slightly larger than the volume of solid Ar extracted from shock and diamond-anvil measurements at similar pressures (19 cm³/mol, Ross et al., 1986; Zha et al., 1986) and smaller than the volume of Ar vapor at these pressures calculated by the Redlich-Kwong equation and corresponding states (32.5 cm³/mol). Despite the large uncertainties in the enthalpies of solution, our calculated values are within the range for Ar in magmas at 1 bar (Lux, 1987) and for CO_2 at high pressure (Stolper et al., 1987). The calculated solubility of Ar in basalt at 1 atm compares well with the data of Hayatsu and Waboso (1985). Figure 10 shows the best-fit solution to Equation 4 superimposed on the data from Figure 5.

Freezing-point depression

So far we have assumed that Ar dissolves in an energetically inert fashion and that the solution is an ideal mixture of Ar and oxygen atoms. For simplicity, we cal-

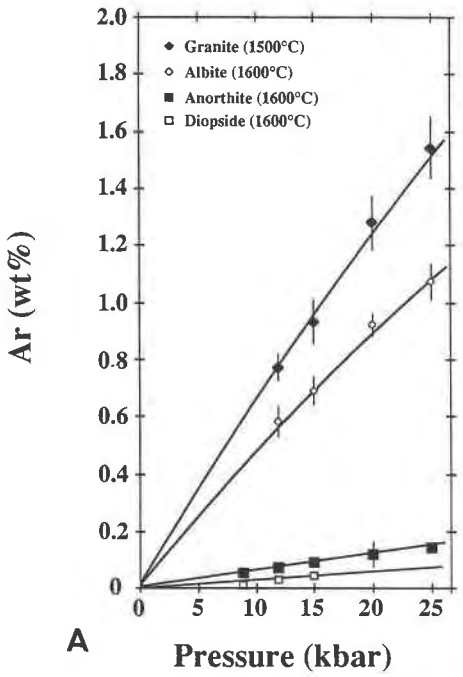

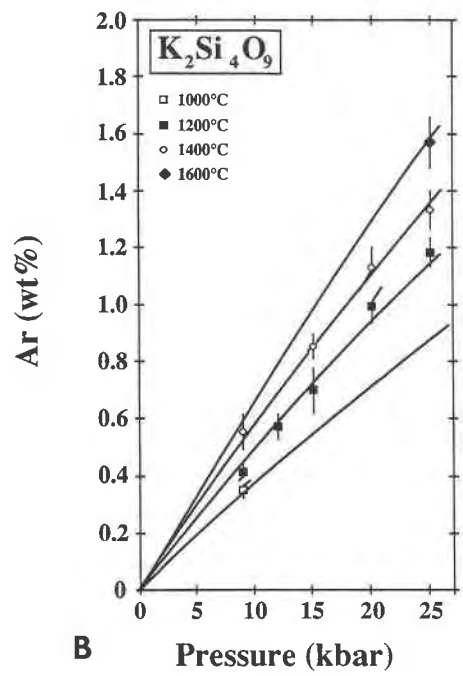

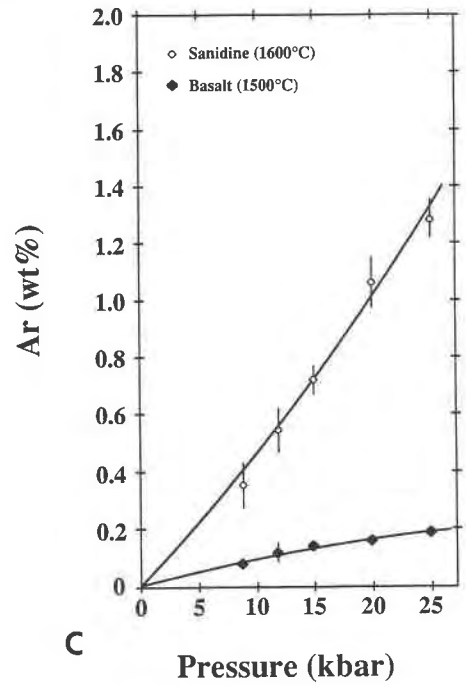

Fig. 10. Concentration of Ar vs. pressure. Curves represent the calculated solutions to Eq. 4.

culated the temperature of the Ar-saturated solidus under the most ideal conditions of solution, simple solute dilution. This can be tested by experimental determination of the solid-liquid-vapor equilibria.

Figure 11 illustrates the extremely different energetic effects of H_2O, CO_2, and Ar in $KAlSi_3O_8$ liquid. Despite the high solubility of Ar in $KAlSi_3O_8$ liquid relative to that in the other compositions, Ar depresses the freezing point of sanidine only ~10 °C at 5 kbar, ~30 °C at 12 kbar, and ~20 °C at 20 kbar. This contrasts sharply with the depression of the solidus of ~30 °C, ~140 °C, and ~170 °C that CO_2 saturation produces at 5, 12, and 20 kbar, respectively, and a freezing-point depression of >300 °C that H_2O produces at pressures greater than 5 kbar. Equation 4 was used to calculate X_{Ar} (defined in the previous section) at the pressure and temperature of the solidus, and the high-pressure values for the enthalpy of fusion are from Boettcher et al. (1982) for albite and diopside, and from Robie et al. (1978) for anorthite and sanidine. The small measured decrease in the melting point of sanidine is consistent with a simple calculation based on the colligative properties of the solute-solvent interaction, where the solute is solely a diluent and the solvent is insensitive to the chemical characteristics of the solute molecule (Atkins, 1978). The data in Table 3 show that Ar is ineffective in depressing the freezing point of diopside and anorthite, consistent with the calculations, supporting the assumption that Ar is dissolving as an atomic species in simple silicate liquids.

Table 4. Best-fit parameters from Eq. 4

	P^o (kbar)	T^o (°C)	X^0_{Ar}	ΔH^0_{Ar} (kJ/mol)	V^0_{Ar} (cm³/mol)
$NaAlSi_3O_8$	15	1600	0.0057 ± 0.0004	8.2 ± 0.8	22.8 ± 0.3
$KAlSi_3O_8$	15	1600	0.0063 ± 0.0004	7.2 ± 1.0	20.6 ± 0.3
$CaAl_2Si_2O_8$	15	1600	0.0008 ± 0.0001	14.1 ± 6.2	22.5 ± 0.5
$CaMgSi_2O_6$	15	1600	0.0004 ± 0.0001	14.3 ± 6.5	21.5 ± 0.6
$K_2Si_4O_9$	15	1400	0.0079 ± 0.0004	12.0 ± 0.8	22.6 ± 0.3
Granite	15	1600	0.0081 ± 0.0009	9.3 ± 0.5	23.1 ± 0.3
Basalt	15	1600	0.0012 ± 0.0002	12.9 ± 6.0	23.7 ± 0.5

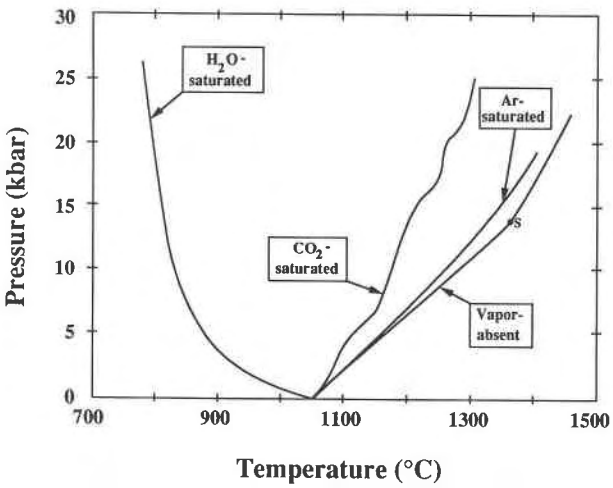

Fig. 11. Pressure-temperature projection of the solidi of sanidine, sanidine + Ar, sanidine + CO_2, and sanidine + H_2O. The vapor-absent solidus is from Boettcher et al. (1984), the CO_2-saturated solidus is from Boettcher et al. (1987), and the H_2O-saturated solidus is from Lambert et al. (1969) and Huang and Wyllie (1975). At pressures above the singular point, *S*, sanidine melts congruently.

Unlike in the sanidine-CO_2 and sanidine-Ar systems, the albite-Ar and albite-CO_2 solidi (Boettcher et al., 1987) are in close agreement, suggesting that CO_2 in albite liquid is predominantly in molecular form at high pressure (Boettcher et al., 1987). This observation supports the predictions of Boettcher et al. (1987) that CO_2 more effectively depolymerizes $KAlSi_3O_8$ liquid than $NaAlSi_3O_8$ liquid, possibly because of the greater stability of K_2CO_3 relative to Na_2CO_3 in silicate liquids. Spectroscopic observations of $KAlSi_3O_8$-CO_2 glass and measurements of the effects of Ar and CO_2 on the viscosity as a function of pressure will be helpful in corroborating these predictions.

Discussion

Compositional dependence of Ar concentration

Figures 5 to 9 show that the solubility of Ar at constant pressure is a strong function of the liquid composition. It is tempting to attribute these differences in solubility to structural characteristics of the liquid on an atomic scale. Unfortunately, the low concentration of Ar, or of any large molecular volatile species such as CO_2, precludes the tentative assignment of available sites to quasi-crystalline structural entities in the liquid. For example, the relatively high concentration of Ar in $KAlSi_3O_8$ corresponds to 1 Ar atom per ~80 oxygen atoms (25 kbar). In a hypothetical situation where the structure of the liquid is identical to that of its crystalline analogue, this is equivalent to 1 Ar atom in every 3 crystallographic unit cells. $NaAlSi_3O_8$ yields roughly the same concentration, whereas $CaMgSi_2O_6$ only has 1 Ar atom per ~150 unit cells. If the atoms are distributed in pairs or triplets (Angell et al., 1988), the concentration of sites is even more dilute. Although albite and anorthite, for example, have similar structures in the crystalline state, their liquid structures are very different (Taylor and Brown, 1979). These differences indicate the profound influence of different network-forming and network-modifying cations on the structure of the liquid, and they are reflected in the variations in the solubility of Ar and other physical properties.

Despite the low solubility of Ar, there are systematic compositional trends. Highly polymerized liquids (feldspars and granite) have the highest solubilities, with the exception of $CaAl_2Si_2O_8$, which has a very low solubility. However, adding SiO_2 to $CaAl_2Si_2O_8$ results in a rapid increase in the Ar concentration (Fig. 8). Interestingly, along the anorthite-quartz join and the plagioclase join (Fig. 7), where NBO/T is 0, equivalent values of Al/Si yield similar Ar concentrations. In addition, the concentration of Ar remains nearly invariant in the alkali feldspars (with constant Al/Si), suggesting that Al/Si in the tetrahedral framework structure influences the solubility.

With Raman spectroscopy, Seifert et al. (1982) noted that when Al_2O_3 was added to silicates with monovalent cations to charge-balance tetrahedral Al^{3+}, a bimodal distribution of ring sizes was created in the liquid (glass). An increase in Al/Si produced a decrease in the average intertetrahedral bond angles, and hence a decrease in the average ring size in the glass, which would tend to inhibit the solubility of Ar based on the observed compositional trends. Alternatively, adding Al_2O_3 to liquids with divalent charge-balancing cations (Ca, Mg) resulted in three types of rings: six-membered rings with no Al^{3+}, four-membered rings with Al/Si = 1, and six-membered rings with no Si^{4+}. Because Ar is more soluble in highly polymerized liquids with low Al/Si, it is plausible that Ar preferentially enters the six-member, Si^{4+}-only sites in liquids with high Al/Si. The low concentration of Ar in anorthite liquid may reflect a low concentration of Si^{4+} rings relative to rings with some Al^{3+}, which inhibits the solubility.

Adding CaO and MgO to SiO_2 (McMillan, 1984) or $CaMgSi_2O_6$ component to $NaAlSi_3O_8$ depolymerizes the liquid and creates a structure dominated by tetrahedral chains. Concomitantly, there is a large decrease in the concentration of Ar. Combining the above with the observation that adding Al to the tetrahedral network produces a decrease in solubility suggests that the probability of an Ar atom finding a suitable site within the liquid structure depends on the amount of units or clusters within the liquid that have a low concentration of nonbridging oxygens and contain predominantly Si. A plot of the mole fraction of SiO_2 for all our liquids vs. the concentration of Ar reveals that increasing SiO_2 dramatically enhances solubility (Fig. 12).

Other physical properties of the liquids, notably viscosity, are derivative of the chemical and structural parameters noted above. Adding $CaAl_2O_4$ to liquid SiO_2 decreases the viscosity by several orders of magnitude

(Kushiro, 1981), as does adding $CaMgSi_2O_6$ to $NaAlSi_3O_8$ (Scarfe and Cronin, 1985; Brearley et al., 1986). Among the feldspathic liquids, $KAlSi_3O_8$ is the most viscous, closely followed by albite, with anorthite being by far the most fluid (Urbain et al., 1982; Scarfe, 1986, provides a review). The viscosities of intermediate-composition liquids along these joins show negative deviations from ideal mechanical mixtures of the two end-members; similar negative deviations occur in the plots of Ar concentration vs. composition (Figs. 7 to 9). The concentrations of Ar generally correlate positively with viscosities, but $K_2Si_4O_9$ has a viscosity that is substantially lower than other silica-rich compositions that have high solubilities of Ar (Dickinson and Scarfe, 1985). Apparently, the high concentration of polymeric SiO_2 units outweighs the slight depolymerization (and subsequent decrease of viscosity) caused by K in the absence of network-forming Al^{3+}.

Kinetic entrapment of the Ar, controlled by the rheologic properties of the liquid, may be discounted as an explanation for the compositional dependence of the Ar concentration for two reasons. First, under isobaric conditions, the viscosities of silicate liquids are strongly correlated with decreasing temperature (Urbain et al., 1982). Nowhere in our study does the solubility of Ar decrease with increasing temperature, although our data cover at least a 200 °C range for most compositions, which decreases the viscosity by more than two orders of magnitude (Scarfe, 1986). In $K_2Si_4O_9$, the concentration of Ar isobarically increases with temperature. Second, the viscosities of fully polymerized liquids such as molten albite, sanidine, or granite, with Al/Si < 1, have negative pressure dependences, whereas the viscosities of relatively depolymerized liquids such as molten diopside have a positive pressure dependence (Brearley et al., 1986; Scarfe et al., 1987). With increasing pressure, the negative difference between the molar volume of the Ar in the vapor and that in solution favors dissolution, but decreasing viscosity favors exsolution. Because viscosity increases in $CaMgSi_2O_6$ liquid with increasing pressure (Scarfe et al., 1987), if these effects operate together, this would produce a more pronounced pressure dependence of the solubility of Ar than for more polymerized liquids. Figure 5 reveals that this is not the case.

Knowledge of the effect of Ar on the viscosity of silicate liquids will further our understanding of the changes in the liquid structure attending the solution of molecular volatile species. On the basis of the work of Dingwell (1987), Brearley and Boettcher (1986), and White and Montana (in preparation) on the effects of H_2O, F, and CO_2, respectively, we predict that Ar will have a minor effect on the fluid properties of liquids at high pressure because of the inert nature of the dissolution.

Pressure and temperature dependence

The solubility of Ar displays a positive pressure dependence in all of the liquid compositions studied (Fig. 5). For example, in $NaAlSi_3O_8$ liquid at 1500 °C, the solubility of Ar increases from 0.42 ± 0.04 wt% at 9 kbar to 1.11 ± 0.07 wt% at 25 kbar. Within the uncertainty of our analytical technique, the solubility of Ar is independent of temperature (e.g., Fig. 6A), with the exception of $K_2Si_4O_9$, which shows a positive temperature dependence between 1000 and 1600 °C (Fig. 6B). We do not have a convincing explanation why this effect is not observed in the other liquids, but a large positive enthalpy of solution and increasing solubility with increasing temperature is consistent with the solubility of Ar at atmospheric pressure in molten silicates (e.g., Lux, 1987), in water (Ozima and Podosek, 1983, although the enthalpy of solution is negative in cold water), and in molten fluorides (Blander et al., 1959). The temperature independence of the solubility of Ar may reflect the large atomic radius of Ar and the considerable energy required to move such a species from one site to another within the liquid structure (Stolper et al., 1987).

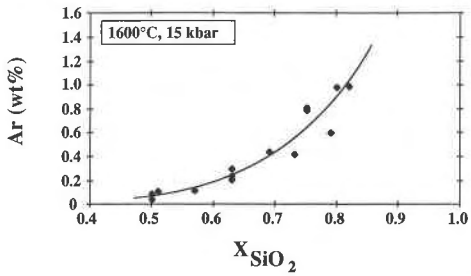

Fig. 12. Concentration of Ar in glasses vs. mole fraction of SiO_2 for all liquid compositions. Error bars have been omitted for clarity.

In the free-volume theory of Doremus (1966), the solvent has a limited volume in which the solute can dissolve. This is often expressed mathematically as

$$V_f = 1 - (V_0/V) \quad (5)$$

where V_f is the free volume, V is the molar volume of the liquid or glass, and V_0 is the close-packed molar volume of the atoms. The fraction of the free volume that is accessible to the dissolving species depends on the structure of the liquid, and because different combinations of ions result in different structural arrangements, two liquids could have the same molar volume but have different available free volumes. However, this equation provides the intuitively satisfying result that free volume, and consequently the solubility of an inert or molecular species in a liquid, is inversely correlated with the density of the liquid and the radius of the solute. Both of these predictions are supported by experimental determinations of the solubilities of noble gases at low pressure (e.g., Blander et al., 1959; Grimes et al., 1959; Kirsten, 1968; Lux, 1987).

To test the hypothesis that the solubility of Ar is inversely correlated with the density of the solvent at high pressures, we calculated the density of our liquids at 15 kbar and 1600 °C (Fig. 13) with the Birch-Murnaghan equation of state. One-bar volumes and thermal expan-

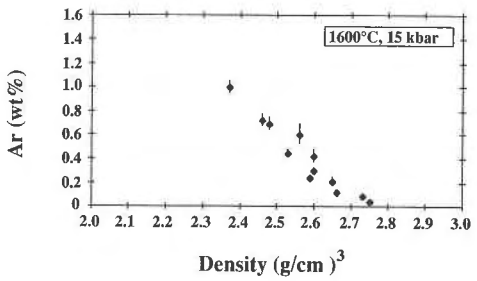

Fig. 13. Concentration of Ar vs. densities of liquids (calculated from the Birch-Murnaghan equation of state).

sivities are those of Lange and Carmichael (1987), and isothermal bulk moduli are from Herzberg (1987). The pressure dependence of the bulk modulus (K') was set equal to 6, which is an average value for silicate liquids (e.g., Rigden et al., 1988). Given the uncertainties in such a large extrapolation of density in P-T space, our high-pressure data seem to adequately retain the correlation between density and Ar solubility. The density of liquid SiO_2 at 1600 °C and 15 kbar is calculated to be 2.44 g/cm^3. If the above correlation between density and solubility of Ar holds, the concentration of Ar in liquid SiO_2 at these conditions would be less than that in $K_2Si_4O_9$. However, because the model of Lange and Carmichael is based on a limited compositional range, the value for the partial molar volume of SiO_2 may not be valid. Extrapolating the data of Bacon et al. (1960) produces a value of 28.15 cm^3/mol for V_{SiO_2}, which corresponds to a density of 2.33 g/cm^3 at 15 kbar. Here, the concentration of Ar dissolved in liquid SiO_2 is greater than in $K_2Si_4O_9$, consistent with our extrapolations. The large isobaric thermal expansivity of K_2O relative to the other oxide components produces a large decrease in the density of $K_2Si_4O_9$, which may partially explain the positive temperature dependence of the solubility of Ar in this composition.

The free volume is also given directly by X_g/ρ_v, where X_g is the concentration of the gas in the glass and ρ_v is the density of the vapor (Doremus, 1966). At low pressures, where Henry's law is obeyed, this ratio, and hence the free volume, is constant, and a plot of X_g vs. ρ_v is a straight line. One corollary of Equation 5 is that the large isothermal compressibility of the bulk sample relative to V_0 will result in a decrease in the free volume of the sample with increasing pressure. This predicts that a pressure will be reached where the positive pressure dependence from Henry's law is overrun by the effect of the shrinking available free volume, producing a decrease in X_g/ρ_v. This decrease will appear as an asymptotic approach to a limiting saturation concentration on a plot of X_g vs. ρ_v. Larger species such as Ar would achieve the maximum solubility at lower pressures than smaller species such as He and Ne (Doremus, 1966). Figure 14 plots the concentration of Ar in $KAlSi_3O_8$ glass at 1600 °C as a function of gas density. The rapid increase in X_g/ρ_v demonstrates that this ratio does not sufficiently represent the free volume because of nonideality of the vapor at these pressures. Because we lack low-pressure data, it is impossible to comment on the applicability of this theory at lower pressures where the vapor is more nearly ideal. Shelby (1976) observed an increase in X_g/ρ_v for He and Ne in silica glass at pressures below 1.4 kbar, indicating that this ratio is being controlled more by the incompressibility of the solute than by the compressibility of the solvent at pressures well below those of this study. Our data, and those of Shelby (1976) and Carroll and Stolper (1987) show that the solubility of a volatile as a function of pressure cannot be adequately described using X_g/ρ_v to define the free volume.

An alternative to the free-volume approach is the Langmuir adsorption model (Barrer and Vaughan, 1967), given by $X_g = YKf/(Y + Kf)$, where K is the solubility coefficient or Henry's law constant, Y is the saturation concentration, and f is the fugacity of the solute component in the vapor. At low fugacities, where Kf is much smaller than Y, the concentration, X_g, is given by Henry's law, whereas at higher fugacities, the concentration of the solute asymptotically approaches Y as the solvent achieves the maximum saturation solubility. Figure 15 illustrates that a plot of the solubility of Ar in $KAlSi_3O_8$ at 1600 °C vs. the fugacity of the gas has the form of a Langmuir-type curve. However, we are hesitant to interpret this as an indication that the concentration of Ar is approaching a limiting value. The trend in Figure 5 does not indicate that the Ar concentration is reaching a maximum, and increasing the pressure will probably result in a nearly linear increase in solubility, for all compositions. We ascribe the form of the curve in Figure 15 to the dominating effect of the rapidly increasing fugacity coefficients of Ar on the shape of the curve at these pressures, and we do not interpret this as evidence of an asymptotic approach to maximum saturation. Because of the inferred low solubilities of the larger noble gases Xe and Kr, it will be illustrative to determine if the concentrations of these gases in silicate liquids achieve a maximum in the pressure range of this study.

Comparison with previous results

There are several conceivable reasons why the concentrations of Ar in $K_2Si_4O_9$ liquid reported here are at least an order of magnitude less than that measured by Faile and Roy (1966) at a similar pressure (9.5 vs. 9 kbar). They used Ar gas as the pressure medium and obtained Ar concentrations by weighing the sample and capsule assembly before and after the experiment, attributing the weight gain to dissolved Ar. This gain includes all contaminants in the sample and capsule, as well as Ar in bubbles (we observe bubbles in this glass) or adsorbed onto the surface of the grains and the capsule walls. Lux (1987), using mass spectrometry, found that the concentration of light noble gases was a function of the surface area of the sample. Although the concentrations of Ar are considerably higher in the study of Faile and Roy than

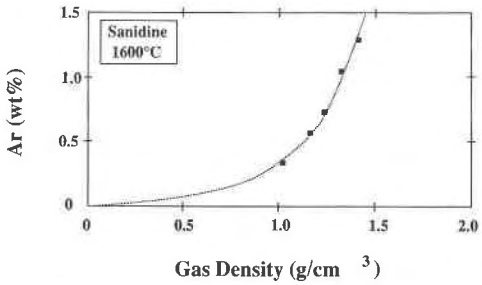

Fig. 14. Concentration of Ar vs. density of Ar gas for $KAlSi_3O_8$ liquid at 1600 °C.

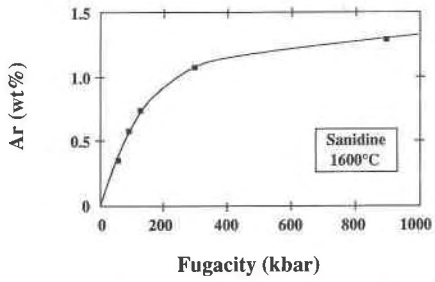

Fig. 15. Concentration of Ar vs. fugacity of Ar gas for $KAlSi_3O_8$ liquid at 1600 °C.

in Lux's study, the contribution from contaminants not detected by a mass spectrometer and the added surface area of the capsule may decrease the analytical accuracy. This might help explain why their solubilities display a second derivative with respect to pressure that is much more highly negative than ours. Also, the starting glasses of Faile and Roy (1966) were prepared by fusion in the atmosphere, and experiments were conducted in open capsules (800 °C), probably resulting in depletion of K, driving the composition toward SiO_2, and enhancing the solubility of Ar. An assessment of this effect is precluded by the absence of postrun analyses of the glasses.

Carroll and Stolper (1987) measured 0.45 wt% Ar in SiO_2 glass at 2.8 kbar using an electron-microprobe technique and a calibration curve similar to the one described here. These results agree reasonably well with the plot of Ar concentration along the $CaAl_2Si_2O_8$-SiO_2 join (Fig. 8) and the plot of Ar vs. SiO_2 (Fig. 12). Also, the calculated solubility of Ar in tholeiitic basalt at 1 bar (Eq. 4) is consistent with the data of Hayatsu and Waboso (1985) and Lux (1987), considering the difference in basalt compositions.

The absence of a suitable standard will draw into question the accuracy of our absolute concentrations. The strong internal consistency of our data set and the day-to-day reproducibility of our results give us confidence in our determinations. An Ar-bearing sample that has been well calibrated by another analytical method will be a valuable contribution to future work.

A comparison of the solubility of Ar with that of CO_2 and H_2O

A direct comparison of the solubility of an inert atomic species, e.g., Ar, with a reactive molecular species is only meaningful in a qualitative sense. However, some general observations and conclusions can be drawn from a comparison of the compositional dependence of the solubility of H_2O, CO_2, and Ar in silicate liquids at high pressure. Several investigators have measured the solubility of CO_2 as a function of pressure, temperature, and composition (e.g., Mysen and Virgo, 1980a, 1980b; Fine and Stolper, 1985; Stolper et al., 1987). Fine and Stolper (1985) observed that the ratio of molecular CO_2 to CO_3^{2-} increases with increasing silica content along the SiO_2-$NaAlO_2$ join. This is in accord with our trend of increasing Ar with increasing SiO_2 (Fig. 12). Furthermore, the low solubility of molecular CO_2 in depolymerized liquids (e.g., Mysen, 1976; Fine and Stolper, 1986) supports the observation that the solubility mechanisms of molecular CO_2 and Ar are similar. The absolute concentrations of molecular CO_2 in albitic liquid reported by Stolper et al. (1987) are similar to ours for Ar, although they found a slight negative temperature dependence of the solubility of molecular CO_2, whereas for Ar, we see none. The apparent similarity in the systematics of the solubility of these species suggests that there is a site within the liquid that is suitable for CO_2 and Ar. We speculate that this site is associated with highly polymerized silicate anionic units with a low Al/Si.

In stark contrast, the solubility of H_2O is much greater than that of Ar or CO_2 at high pressures (McMillan and Holloway, 1987), and the solubility mechanisms of H_2O in silicate liquids are complex (Mysen and Virgo, 1986; McMillan and Holloway, 1987). Stolper (1982a) and Silver (1988) showed that the concentration of molecular H_2O increases with increasing total dissolved H_2O, eventually predominating over hydroxyl groups at high H_2O contents. Silver (1988) concluded that the speciation of H_2O in the range of compositions in her study is approximately independent of composition. This suggests that in liquids that exhibit a high solubility of H_2O, the dominant species will be molecular H_2O. Because we are interested in a comparison of molecular species, we restrict our discussion to higher pressures on the assumption that this relationship holds for all compositions at >10 kbar.

In fully polymerized sodium aluminosilicate liquids, the solubility of H_2O generally increases with increasing $NaAlO_2$ content, in contrast to the dissolution of CO_2 and Ar (see Fig. 6 in McMillan and Holloway, 1987). Although this relationship is not as clear on either the $KAlO_2$-SiO_2 or $CaAl_2O_4$-SiO_2 joins, H_2O (and more importantly, in this case, molecular H_2O) appears to be associated with sodium aluminosilicate (or even aluminate) anionic units in the liquid. Less polymerized liquids, such as forsterite and diopside, also exhibit a high bulk solubility of H_2O (Hodges, 1974; Mysen and Virgo, 1986; McMillan and Holloway, 1987), again reflecting the contrasting solubility mechanisms of H_2O vs. Ar and molec-

ular CO_2. Together with the compositional independence of the ratio of molecular H_2O to OH^-, this suggests that the dissolution mechanism of H_2O is not wholly controlled by the tetrahedral framework structure of the liquid. Unlike CO_2 or Ar, H_2O may occupy many sites in the liquid that may not be controlled by structure or the types of cations (Silver, 1988), whereas molecular CO_2 and Ar appear to be associated with SiO_2-rich units in polymerized liquids and are essentially insoluble in very depolymerized liquids.

Acknowledgments

This research was supported by National Science Foundation Grants EAR87-05870 and EAR87-20289 and UCLA Academic Senate Grants to Montana. Robert Jones provided helpful advice and valuable assistance with the operation of the electron microprobe. Scott Boettcher helped with the design, construction, and operation of the glove-box, and John Rice assisted in the construction of the high-pressure cells. Jim Dickinson of Corning Glass and Dave Stewart of the USGS provided us with $KAlSi_3O_8$ glass. Don Peacor and David Moecher of the University of Michigan and Robert Coleman of Stanford University provided the albite. The late Chris Scarfe of the University of Alberta supplied the $CaAl_2Si_2O_8$ glass and the glasses on the join $NaAlSi_3O_8$-$CaMgSi_2O_6$. We benefited from discussions with Wayne Dollase of UCLA, Mike Carroll at the California Institute of Technology, and Jim Dickinson. Richard Arculus provided an official review.

References cited

Angell, C.A., Scamehorn, C.A., Phifer, C.C. Kadiyala, R.R., and Cheeseman, P.A. (1988) Ion dynamics studies of liquid and glassy silicates, and gas-in-liquid solutions. Physics and Chemistry of Minerals, 15, 221–227.

Atkins, P.W. (1978) Physical chemistry, 1018 p. Oxford University Press, Oxford, England.

Bacon, J.F., Hasapis, A.A., and Wholley, J.W., Jr. (1960) Viscosity and density of molten silica and high silica content glasses. Physics and Chemistry of Glasses, 1, 90–98.

Barrer, R., and Vaughan, D.E. (1967) Solution and diffusion of helium and neon in tridymite and cristobalite. Transactions of the Faraday Society, 63, 2275–2290.

Blander, M., Grimes, W.R., Smith, N.V., and Watson, G.M. (1959) Solubility of noble gases in molten fluorides. II. In the LiF-NaF-KF eutectic mixture. Journal of Physical Chemistry, 63, 1164–1167.

Boettcher, A.L. (1970) The system CaO-Al_2O_3-SiO_2-H_2O at high pressures and temperatures. Journal of Petrology, 11, 337–379.

——— (1984) The system SiO_2-H_2O-CO_2: Melting, solubility mechanisms of carbon, and liquid structure to high pressures. American Mineralogist, 69, 823–833.

Boettcher, A.L., and Wyllie, P.J. (1968) Melting of granite with excess water to 30 kilobars pressure. Journal of Geology, 76, 235–244.

——— (1969) Phase relationships in the system $NaAlSiO_4$-SiO_2-H_2O to 35 kilobars pressure. American Journal of Science, 267, 875–909.

Boettcher, A.L., Windom, K.E., Bohlen, S.R., and Luth, R.W. (1981) Low friction, anhydrous, low- to high-temperature furnace sample assembly for piston-cylinder apparatus. Reviews of Scientific Instruments, 52, 1903–1904.

Boettcher, A.L., Burnham, C.W., Windom, K.E., and Bohlen, S.R. (1982) Liquids, glasses, and the melting of silicates to high pressures. Journal of Geology, 90, 127–138.

Boettcher, A.L., Guo, Q., Bohlen, S.R., and Hanson, B. (1984) Melting in feldspar-bearing systems to high pressures and the structure of aluminosilicate liquids. Geology, 12, 202–204.

Boettcher, A.L., Luth, R.W., and White, B.S. (1987) Carbon in silicate liquids: The systems $NaAlSi_3O_8$-CO_2, $CaAl_2Si_2O_8$-CO_2, and $KAlSi_3O_8$-CO_2. Contributions to Mineralogy and Petrology, 97, 297–304.

Bohlen, S.R., Boettcher, A.L., and Wall, V.J. (1982) The system albite-H_2O-CO_2: A model for melting and activities of water at high pressures. American Mineralogist, 67, 451–462.

Brearley, M., and Boettcher, A.L. (1986) The effect of CO_2 on the viscosity of silicate liquids at high pressure (abs.). EOS, 67, 1275.

Brearley, M., Dickinson, J.E., and Scarfe, C.M. (1986) Pressure dependence of melt viscosities on the join diopside-albite. Geochimica et Cosmochimica Acta, 50, 2563–2570.

Broadhurst, C.L., Drake, M.J., Hagee, B.E., and Bernatowicz, T.J. (1988) Solubilities and partitioning of noble gases in mineral melt systems. II. Synthesis experiments for Ne, Ar, Kr, and Xe in anorthite, diopside, forsterite, and coexisting melts. Lunar and Planetary Science Letters, 19, 138–139.

Carroll, M.R., and Stolper, E.M. (1987) Ar solubility and diffusion in silica glass. Geological Society of America Abstracts with Programs, 19, 612.

Chao, K.C., and Greenkorn, R.A. (1968) Thermodynamics of fluids, 298 p. Marcel Decker, New York.

Dickinson, J.E., and Scarfe, C.M. (1985) Pressure-induced structural changes in $K_2Si_4O_9$ silicate melt (abs.). EOS, 66, 395.

Dingwell, D.B. (1987) Melt viscosities in the system $NaAlSi_3O_8$-H_2O-F_2O_{-1}. In B.O. Mysen, Ed., Magmatic processes: Physiochemical principles, p. 423–432. Geochemical Society, University Park, Pennsylvania.

Doremus, R.H. (1966) Physical solubility of gases in fused silica. Journal of the American Ceramic Society, 49, 461–462.

——— (1973) Glass science, 349 p. Wiley, New York.

Dymond, J., and Hogan, L. (1973) Noble gas abundance patterns in deep-sea basalts—Primordial gases from the mantle. Earth and Planetary Science Letters, 20, 131–139.

Eggler, D.H. (1978) The effect of CO_2 on the partial melting of peridotite in the system Na_2O-CaO-Al_2O_3-MgO-SiO_2-CO_2 to 35 kb with an analysis of melting in a peridotite-H_2O-CO_2 system. American Journal of Science, 278, 305–343.

Eggler, D.H., and Rosenhauer, M. (1978) Carbon dioxide in silicate melts: II. Solubilities of CO_2 and H_2O in Al_2O_3 (diopside) liquids and vapors to pressures to 40 kb. American Journal of Science, 278, 64–91.

Faile, S.P., and Roy, D.M. (1966) Solubilities of Ar, N_2, CO_2, and He in glasses at pressures to 10 kbars. Journal of the American Ceramic Society, 49, 638–643.

Ferry, J.M., and Baumgartner, L. (1987) Thermodynamic models of molecular fluids at the elevated pressures and temperatures of crustal metamorphism. Mineralogical Society of America Reviews in Mineralogy, 17, 323–365.

Fine, G., and Stolper, E. (1985) The speciation of carbon dioxide in sodium aluminosilicate glasses. Contributions to Mineralogy and Petrology, 91, 105–121.

——— (1986) Dissolved carbon dioxide in basaltic glasses: Concentrations and speciation. Earth and Planetary Science Letters, 76, 263–278.

Flanagan, F.J. (1973) 1972 values for international geochemical reference samples. Geochimica et Cosmochimica Acta, 37, 1189–1200.

Goldsmith, J.R. (1980) The melting and breakdown reactions of anorthite at high pressures and temperatures. American Mineralogist, 65, 272–284.

Goranson, R.W. (1938) Silicate-water systems: Phase equilibria in the $NaAlSi_3O_8$-H_2O and $KAlSi_3O_8$-H_2O systems at high temperatures and pressures. American Journal of Science, 35-A, 71–91.

Greenwood, N.N., and Earnshaw, A. (1984) Chemistry of the elements, 1542 p. Pergamon, Oxford, England.

Grimes, W.R., Smith, N.V., and Watson, G.M. (1959) Solubility of noble gases in molten fluorides. I. In mixtures of NaF-ZrF_4 (53–47 mole%) and NaF-ZrF_4-UF_4 (50–46–4 mole%). Journal of Physical Chemistry, 62, 862–866.

Hayatsu, A., and Waboso, C.E. (1985) The solubility of rare gases in silicate melts and implications for K-Ar dating. Chemical Geology, 52, 97–102.

Herzberg, C.T. (1987) Magma density at high pressure. Part 1: The effect of composition on the elastic properties of silicate liquids. In B.O. Mysen, Ed., Magmatic processes: Physiochemical principles, p. 25–46. Geochemical Society, University Park, Pennsylvania.

Hiyagon, H., and Ozima, M. (1982) Noble gas distribution between basalt melt and crystals. Earth and Planetary Science Letters, 58, 255–264.

——— (1986) Partition of noble gases between olivine and basalt melt. Geochimica et Cosmochimica Acta, 50, 2045–2058.

Hodges, F.N. (1974) The solubility of H_2O in silicate melts. Carnegie Institution of Washington Year Book 73, 251–255.

Holloway, J.R. (1977) Fugacity and activity of molecular species in supercritical fluids. In D.G. Fraser, Ed., Thermodynamics in geology, p. 161–181. Reidel, Boston.

Huang, W.L., and Wyllie, P.J. (1975) Melting relations in the system $NaAlSi_3O_8$-$KAlSi_3O_8$-SiO_2 to 35 kilobars, dry and with excess water. Journal of Geology, 83, 737–748.

Jambon, A., Braun, O., and Weber, H. (1982) Solubility of noble gases in a basalt melt, preliminary results at 1300 °C, 1 bar (abs.). EOS, 63, 451.

Kirsten, T. (1968) Incorporation of rare gases in solidifying enstatite melts. Journal of Geophysical Research, 73, 2807–2810.

Kirsten, T., Richter, H., and Storzer, D. (1981) Abundance patterns of rare gases in submarine basalt and glasses (abs.). Meteoritics, 16, 341.

Kuroda, P.K., Sherrill, R.D., and Jackson, K.C. (1977) Abundances and isotopic compositions of rare gases in granites. Geochemical Journal, 11, 75–90.

Kushiro, I. (1975) On the nature of silicate melt and its significance in magma genesis: Regularities in the shift of the liquidus boundaries involving olivine, pyroxene, and silica minerals. American Journal of Science, 275, 411–431.

——— (1981) Change in viscosity with pressure of melts in the system CaO-Al_2O_3-SiO_2. Carnegie Institute of Washington Year Book 80, 339–341.

Lambert, I.B., Robertson, J.K., and Wyllie, P.J. (1969) Melting reactions in the system $KAlSi_3O_8$-SiO_2-H_2O to 18.5 kilobars. American Journal of Science, 267, 609–626.

Lange, R.A., and Carmichael, I.S.E. (1987) Densities of Na_2O-K_2O-CaO-MgO-FeO-Fe_2O_3-Al_2O_3-TiO_2-SiO_2 liquids: New measurements and derived partial molar properties. Geochimica et Cosmochimca Acta, 51, 2931–2946.

Luth, R.W., and Boettcher, A.L. (1986) Hydrogen and the melting of silicates. American Mineralogist, 71, 264–276.

Luth, W.C., and Ingamells, C.O. (1965) Gel preparation of starting materials for hydrothermal experimentation. American Mineralogist, 50, 255–258.

Lux, G. (1987) The behavior of noble gases in silicate liquids: Solution, diffusion, bubbles, and surface effects, with applications to natural samples. Geochimica et Cosmochimica Acta, 51, 1549–1560.

McMillan, P.F. (1984) A Raman spectroscopic study of glasses in the system CaO-MgO-SiO_2. American Mineralogist, 69, 645–659.

McMillan, P.F., and Holloway, J.R. (1987) Water solubility in aluminosilicate melts. Contributions to Mineralogy and Petrology, 97, 320–332.

Mysen, B.O. (1976) The role of volatiles in silicate melts: Solubility of carbon dioxide and water in feldspar, pyroxene, and feldspathoid melts to 30 kb and 1625 °C. American Journal of Science, 276, 969–996.

Mysen, B.O., and Boettcher, A.L. (1976) Melting of a hydrous mantle: III. Phase relations of garnet websterite + H_2O at high pressures and temperatures. Journal of Petrology, 17, 1–14.

Mysen, B.O., and Virgo, D. (1980a) Solubility mechanisms of carbon dioxide in silicate melts: A Raman spectroscopic study. American Mineralogist, 65, 885–899.

——— (1980b) The solubility behavior of CO_2 in melts on the join $NaAlSi_3O_8$-$CaAl_2Si_2O_8$-CO_2 at high pressures and temperatures: A Raman spectroscopic study. American Mineralogist, 65, 1166–1175.

——— (1986) Volatiles in silicate melts at high pressure and temperature. 1. Interaction between OH groups and Si^{4+}, Al^{3+}, Ca^{2+}, Na^+ and H^+. Chemical Geology, 57, 303–331.

Mysen, B.O., Virgo, D., and Seifert, F.A. (1982) The structure of silicate melts: Implications for chemical and physical properties of natural magma. Reviews of Geophysics and Space Physics, 20, 353–383.

Oxtoby, S., and Hamilton, D.L. (1978) The discrete association of water with Na_2O and SiO_2 in NaAl silicate melts. Contributions to Mineralogy and Petrology, 66, 185–188.

Ozima, M., and Podosek, F.A. (1983) Noble gas geochemistry, 367 p. Cambridge University Press, Cambridge, England.

Ozima, M., and Zashu, S. (1983) Noble gases in submarine pillow volcanic glasses. Earth and Planetary Science Letters, 62, 24–40.

Rigden, S.M., Ahrens, T.J., and Stolper, E.M. (1988) Shock compression of molten silicate: Results for a model basaltic composition. Journal of Geophysical Research, 93, 367–382.

Robie, R.A., Hemingway, B.S., and Fisher, J.R. (1978) Thermodynamic properties of minerals and related substances at 298.15 K and 1 bar (10^5 pascals) pressure and at higher temperatures. U.S. Geological Bulletin 1452.

Roselieb, K., Rammensee, W., Buttner, H., and Rosenhauer, M. (1988) Solubility and diffusion of rare gases in silicate melts. Terra Cognita, 8, 75.

Ross, M., Mao, H.K., Bell, P.M., and Xu, J.A. (1986) The equation of state of dense Ar: A comparison of shock and static studies. Journal of Chemical Physics, 85, 1028–1033.

Scarfe, C.M. (1986) Viscosity and density of silicate melts. In C.M. Scarfe, Ed., Silicate melts: Their properties and structure applied to problems in geochemistry, petrology, economic geology, and planetology, p. 36–56. Mineralogical Association of Canada Short Course Handbook 12.

Scarfe, C.M., and Cronin, D.J. (1985) Viscosity-temperature relationships of melts at 1 atm in the system diopside-albite. American Mineralogist, 71, 767–771.

Scarfe, C.M., Mysen, B.O., and Virgo, D. (1987) Pressure dependence of the viscosity of silicate melts. In B.O. Mysen, Ed., Magmatic processes: Physiochemical principles, p. 59–67. Geochemical Society, University Park, Pennsylvania.

Seifert, F., Mysen, B.O., and Virgo, D. (1982) Three-dimensional network structure of quenched melts (glass) in the systems SiO_2-$NaAlO_2$, SiO_2-$CaAl_2O_4$, and SiO_2-$MgAl_2O_4$. American Mineralogist, 67, 696–717.

Shaw, H.R. (1963) Obsidian-H_2O viscosities at 1000 and 2000 bars in the temperature range 700 to 900 °C. Journal of Geophysical Research, 68, 6337–6343.

Shelby, J.E. (1972) Helium migration in natural and synthetic vitreous silica. Journal of the American Ceramic Society, 55, 61–64.

——— (1974) Helium diffusion and solubility in K_2O-SiO_2 glasses. Journal of the American Ceramic Society, 57, 260–263.

——— (1976) Pressure dependence of helium and neon solubility in vitreous silica. Journal of Applied Physics, 47, 135–139.

Shelby, J.E., and Eagan, R.J. (1976) Helium migration in sodium aluminosilicate glasses. Journal of the American Ceramic Society, 59, 420–425.

Silver, L.A. (1988) Water in silicate glasses. Ph.D. thesis, 310 p. California Institute of Technology, Pasadena, California.

Silver, L.A., and Stolper, E. (1985) A thermodynamic model for hydrous silicate melts. Journal of Geology, 93, 161–178.

Stolper, E. (1982a) Water in silicate glasses: An infrared spectroscopic study. Contributions to Mineralogy and Petrology, 81, 1–17.

——— (1982b) The speciation of water in silicate melts. Geochimica et Cosmochimica Acta, 46, 2609–2620.

Stolper, E., Fine, G., Johnson, T., and Newman, S. (1987) Solubility of carbon dioxide in albitic melt. American Mineralogist, 72, 1071–1085.

Taylor, M., and Brown, G.E. (1979) Structure of mineral glasses: I. The feldspar glasses $NaAlSi_3O_8$, $KAlSi_3O_8$, and $CaAl_2Si_2O_8$. Geochimica et Cosmochimica Acta, 43, 61–75.

Urbain, G., Bottinga, Y., and Richet, P. (1982) Viscosity of liquid silica, silicates, and alumino-silicates. Geochimica et Cosmochimica Acta, 46, 1061–1072.

Zha, C.S., Boehler, R., Young, D.A., and Ross, M. (1986) The Ar melting curve to very high pressures. Journal of Chemical Physics, 85, 1034–1036.

MANUSCRIPT RECEIVED JUNE 30, 1988
MANUSCRIPT ACCEPTED JANUARY 12, 1989